Invited Paper https://doi.org/10.7733/jnfcwt.2020.18.1.1

Electrochemical Impedance Spectroscopy and Cyclic Voltammetry Methods for Monitoring $SmCl_3$ Concentration in Molten Eutectic LiCl-KCl

Michael R. Shaltry[1,*], Kerry N. Allahar[2], Darryl P. Butt[3], Michael F. Simpson[3], and Supathorn Phongikaroon[4]
[1]*Idaho National Laboratory, 775 MK Simpson Blvd, Idaho Falls, Idaho 83402, USA*
[2]*Boise State Univ.,1910 University Drive, Boise, Idaho 83725, USA*
[3]*Univ. of Utah, Department of Materials Science & Engineering, 122 S. Central Campus Dr., Salt Lake City, Utah 84112, USA*
[4]*Virginia Commonwealth Univ., 907 Floyd Ave, Richmond, Virginia 23284, USA*

(Received November 5, 2019 / Revised December 9, 2019 / Approved March 10, 2020)

Molten salt solutions consisting of eutectic LiCl-KCl and concentrations of samarium chloride (0.5 to 3.0 wt%) at 500℃ were analyzed using both cyclic voltammetry (CV) and electrochemical impedance spectroscopy (EIS). The CV technique gave the average diffusion coefficient for Sm^{3+} over the concentration range. Equipped with Sm^{3+} diffusion coefficient, the Randles-Sevcik equation predicted Sm^{3+} concentration values that agree with the given experimental values. From CV measurements; the anodic, cathodic, and half-peak potentials were identified and subsequently used as a parameter to acquire EIS spectra. A six-element Voigt model was used to model the EIS data in terms of resistance-time constant pairs. The lowest resistances were observed at the half-peak potential with the associated resistance-time constant pairs characterizing the reversible reaction between Sm^{3+} and Sm^{2+}. By extrapolation, the Voigt model estimated the polarization resistance and established a polarization resistance-concentration relationship.

Keywords: Molten salt, Electrochemical impedance spectroscopy, Cyclic voltammetry, Concentration, Samarium chloride

*Corresponding Author.
Michael R. Shaltry, Idaho National Laboratory, E-mail: michael.shaltry@inl.gov, Tel: +1-208-526-9420

ORCID

Michael R. Shaltry	http://orcid.org/0000-0003-3639-2651	Kerry N. Allahar	http://orcid.org/0000-0001-8478-0291
Darryl P. Butt	http://orcid.org/0000-0003-4501-8864	Michael F. Simpson	http://orcid.org/0000-0002-0099-0097
Supathorn Phongikaroon	http://orcid.org/0000-0002-2019-0118		

1. Introduction

Electrochemical processing utilizing a high temperature molten salt electrolyte, namely Pyroprocessing, is a widely sought technology for used nuclear fuel processing to recover actinides and minimize radioactive waste [1-7]. To be prepared for a large-scale facility deployment, sensor and accounting technologies have received significant attention to establish material accountability consistent with traditional international safeguard methods [8-13]. Within this system, the electrorefiner (ER) is an electrochemical cell that dissolves used metallic fuel anodically and collects metallic actinides cathodically. The molten salt electrolyte in the ER contains the majority of special nuclear materials in the pyroprocessing system [14-20]. Molten salt electrolyte composition sensors are of interest for safeguards due to the typical accumulation of plutonium and other actinides in this salt.

A variety of methods have been pursued to assess the inventory of elements in the molten electrolyte of the pyroprocessing system [21-40]. Among those, electrochemical methods can form the basis of such sensors, since the various species have different electrochemical properties, and there are electrode materials compatible with the harsh environmental conditions found in the ER. Such electrochemistry-based techniques as cyclic voltammetry (CV) and chronopotentiometry (CP), provide simple yet powerful means to quantify species concentrations in molten salts let alone their traditional usages for identifying electrochemical reactions, and measuring electrochemical properties such as diffusion and activity coefficients. One can find numerous applications of these electrochemical probing techniques to molten salts containing uranium [21-25] as well as species that contribute to the composition of the used fuel; plutonium [22,26], americium [22], lanthanum [22], neodymium [22], samarium [27-30], thorium [31], gadolinium [32], cerium [33-35], erbium [36], and neptunium [22,37].

While the aforementioned techniques rely on direct current (DC), electrochemical impedance spectroscopy (EIS) adopts alternating current (AC). Impedance techniques are useful to a variety of industrial applications, e.g. fuel cells [41], solar salt systems [42] and anti-corrosion coatings [43]. As an analytical tool, via frequency and amplitude control, the EIS measurements provide the frequency domain characterization and a unique electrochemical perspective. For example, EIS methods are valuable for elucidating reactions and associated electrochemical mechanisms at electrode/electrolyte interfaces [44]. More specifically, such parameters as reaction rate constant [45-47], corrosion rate [48-50], electrolyte conductivity [51-54], double-layer capacitance [55,56], and exchange current density [57-59] can be determined by EIS techniques.

A selection of reported applications of EIS for the characterization of electrochemical reactions in LiCl-KCl molten salts used in pyroprocessing applications are briefly described herein. Reddy et al. [60] reported the EIS investigation of uranium chloride in LiCl-KCl eutectic at 435℃. In this application EIS spectra in the range of 0.1 to 65 kHz were obtained at potentials ranging from -0.15 to -1.55 V relative to a Ag/AgCl reference electrode. Four equivalent circuit models were used across the potential range to analyze the EIS data. The analysis focused on qualitatively explaining the diffusion, absorption and charge transfer processes associated with the electrochemical reactions occurring at the working electrode. Ghosh et al. [61] used EIS data to calculate the heterogeneous rate constant associated with the reduction of CeO^{+} at a glassy carbon electrode at 550℃ in $MgCl_2$-NaCl-KCl eutectic. An equivalent circuit was used to determine the charge transfer resistance from an EIS spectrum which had an observable Warburg behavior at frequencies down to 100 Hz. Similarly, Vandarkuzhali et al. [62] used EIS data to calculate the heterogeneous rate constant associated with the reduction of lanthanum at a tungsten electrode at 525℃ in LiCl-KCl using data down to 10 Hz that exemplified a Warburg behavior at -0.25 V. Ferry and Picard [63] investigated the Ti^{4+}/Ti^{3+} reduction at 470℃ by analyzing EIS data with an equivalent circuit and obtaining the rate constant for this reaction.

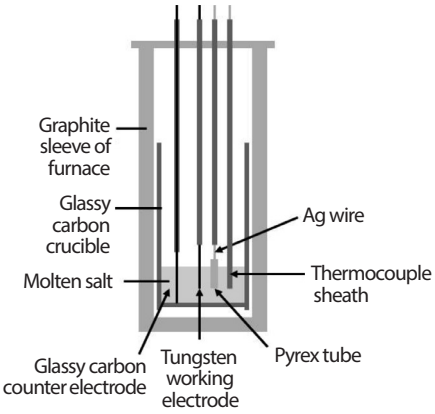

Fig. 1. Shematic of the experimental setup of the three-probe electrode in the molten salt contained in the glassy carbon crucilbe and placed within the sleeve of the furnace.

Although there have been efforts to characterize the electrochemical properties with EIS, to the best of the authors' knowledge, there has been no reported attempt to correlate impedance response to the concentration of a given species in a LiCl-KCl molten salt. The intent of this paper is to introduce the use of EIS for the prescribed purpose. Also provided in this paper is the application of CV technique to estimate the species concentration with the aid of the Randles-Sevcik equation.

To this end, $SmCl_3$ in the range of 0.5 to 3 wt% in LiCl-KCl eutectic was characterized using CV and EIS at 500℃. CV was used to calculate an average diffusion coefficient for Sm^{3+} in the concentration range, while EIS was used to calculate a relationship between polarization resistance and bulk $SmCl_3$ concentration. Comparison of calculated bulk $SmCl_3$ concentrations based on CV and EIS with experimental bulk concentrations demonstrated the applicability of these methods for monitoring concentration changes in LiCl-KCl melts.

In the effort reported here, the Sm^{3+}/Sm^{2+} redox reaction was characterized using EIS. An equivalent circuit composed of a series of resistor-capacitor pairs was used to model spectra. The model was also used to estimate the polarization resistance by extrapolation. The influences of applied potential and $SmCl_3$ concentration were determined by comparing the resistor-time constant pairs and the polarization resistance.

2. Experimental

The experiments were conducted in an MBraun glovebox containing an argon atmosphere with H_2O and O_2 concentrations less than 5 ppm. A Kerr Lab Electro-Melt furnace was located in the glovebox and used to heat the molten salts to 500℃. Eutectic LiCl-KCl salt (99.99%) was obtained from AAPL and anhydrous $SmCl_3$ (99.99%) was obtained from Alfa Aesar. The use of anhydrous salts and under low H_2O and O_2 conditions is meant to minimize the effects of oxide and oxychloride formation in the salt. A tapered cylindrical glassy carbon crucible obtained from HTW Germany was used for containing the salts, which was 16.8 cm in height with a wall thickness of 3 mm. The tapered cylinder had outside diameters of 45 mm and 41 mm at the top and bottom, respectively. The glassy carbon crucible was placed inside the graphite crucible of the furnace.

The electrode assembly consisted of working, counter, and reference electrodes together with a thermocouple for temperature measurement. The working electrode was a 2.0 mm diameter tungsten rod (99.95%, 30 cm in length) obtained from Alfa Aesar. The counter electrode was a 3.0 mm diameter glassy carbon rod (30 cm in length) obtained from HTW Germany. The reference electrode was constructed using a Pyrex tube (10 mm outside diameter and 1.0 mm wall thickness) unto which a Pyrex rod was attached. One end of a 1.0 mm diameter silver wire (99.9%), obtained from Acros Organics, was made into a spiral sufficiently small in diameter to be inserted into the tube. 0.135 g of AgCl beads and 1.00 g of the LiCl-KCl eutectic were placed in the tube. Upon melting, a 5.0 mol% AgCl mixture was obtained that served as the reference electrode. An alumina tube (2 mm and 3 mm inner and outer diameters, respectively) closed at one end was used to sheath the K-type thermocouple.

The electrode assembly was made by placing the working and counter electrodes and the silver wire connect of the reference electrode in alumina tubes of 2 mm and 3 mm inner and outer diameters, respectively, as shown in Fig. 1. The tungsten working electrode was secured in the alumina tube such that 14 mm of it was exposed at one end, the end that would be the working electrode. An alumina paste was used to seal the alumina tube. For the purpose of calculations, the geometric surface area (0.911 cm^2) of the working electrode is used. The glassy carbon counter electrode was not secured in the alumina tube such that it could contact the bottom of the crucible, effectively making the entire crucible the counter electrode.

The CV and EIS experiments were conducted using a Princeton Applied Research VersaSTAT 4-400 potentiostat with VersaStudio software. The electrical leads from the potentiostat were connected to electrical feed-through fittings in the glovebox. The leads from these fittings were connected to the electrodes using alligator clips.

The experimental procedure initiated with mixture preparation. For the first experiment, 80 g of LiCl-KCl eutectic and 0.41 g of $SmCl_3$ were introduced into the crucible, with the mixture comprised of 0.5 wt% (3.23×10^{-5} $mol \cdot cm^{-3}$) $SmCl_3$. The furnace set-point was adjusted to 500℃ with a ramp-rate of 4℃ min^{-1}. Starting from room temperature, this resulted with a heating time of 115 min. The electrode assembly was lowered into the crucible to a position where the working and reference electrodes and thermocouple were approximately 1 cm above the surface of the salt mixture when the furnace temperature was 350℃. At a furnace temperature of 450℃, the salt was assumed to be molten and the electrode assembly was lowered slowly into the melt. Upon contact of the crucible by the glassy carbon counter electrode rod, the assembly was secured in position. The assembly was made such that the exposed end of the working electrode would be totally immersed; approximately 60 % of the Pyrex tube of the reference electrode was also immersed. The thermocouple was immersed to the same extent as the working electrode. The molten salt with electrode assembly immersed was left for 6 h to allow the mixture to become homogeneous before beginning the measurements. This consisted of three scans at a given scan rate (0.1 to 1.5 $V \cdot s^{-1}$).

The EIS experiments were conducted afterwards using the same three-electrode set up with the frequency range of 10 kHz to 0.01 Hz and perturbation amplitude of 10 mV. EIS measurements were acquired at bias potential of -0.84, -0.93 and -1.03 V. Six EIS spectra were acquired at each bias potential. A time period of 1 min was allowed between EIS measurements at the same bias potential while a period of 3 min was allowed when the bias potential was changed. It was found that electrode cleaning steps between measurements was not necessary because the reduced species is soluble. Upon completion of the electrochemical experiments, the furnace was switched off and the electrode assembly was retracted from the molten salt to a position approximately 2 cm above the surface of the melt. The salt was allowed to freeze completely. The experimental procedure was repeated except that only $SmCl_3$ was added to the existing salt mixture to increment its concentration to 1.0 wt% (6.31×10^{-5} $mol \cdot cm^{-3}$), and subsequently to 1.5 (9.47×10^{-5} $mol \cdot cm^{-3}$), 2.0 (1.26×10^{-4} $mol \cdot cm^{-3}$), 2.5 (1.58×10^{-4} $mol \cdot cm^{-3}$) and 3.0 wt% (1.89×10^{-4} $mol \cdot cm^{-3}$). It is noted the concentration of $SmCl_3$ will be presented as wt % in the remainder of this manuscript, however the molar concentration has been provided above for convenience.

3. Results

The CV results associated with the 1.0, 2.0 and 3.0 wt% concentrations of $SmCl_3$ in the eutectic are shown in Fig. 2 where each scan was the third of three scans for a given scan rate.

The potential range of 0 V to -1.6 V was used for the scans in order to observe the reduction of Sm^{3+} to Sm^{2+} and the oxidation of Sm^{2+} to Sm^{3+}. The reduction of Sm^{2+} to Sm occurs at potential more negative than the reduction of Li^+,

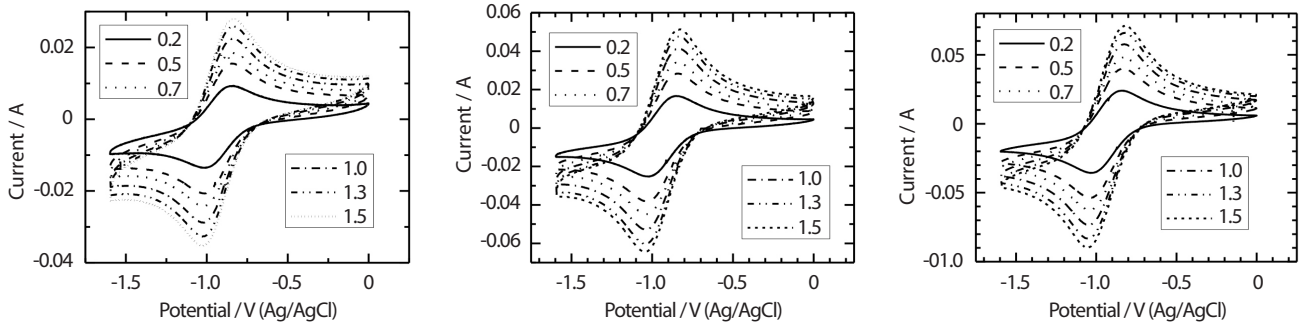

Fig. 2. Cyclic voltammograms for (a) 1 wt%, (b) 2 wt% and (c) 3 wt% $SmCl_3$ in eutectic LiCl-KCl at 500℃ with scan rate in $V \cdot s^{-1}$ as a parameter.

a constituent of the eutectic. The voltammograms consisted of an anodic wave occurring at approximately -0.84 V and a cathodic wave at approximately -1.03 V. There were neither pre-waves nor post-waves associated with either peak. The anodic peak potential, E_p^a, corresponded to the electro-oxidation of Sm^{2+},

$$Sm^{2+} \rightarrow Sm^{3+} + e^- \quad (1)$$

and the cathodic peak potential, E_p^c, the electro-reduction of Sm^{3+},

$$Sm^{3+} + e^- \rightarrow Sm^{2+} \quad (2)$$

Although the experimental conditions were tightly controlled, it is possible that oxide or oxychloride formation occurred, albeit to a very small extent. However, as shown by Fig. 2., there are no unidentified current peaks in the CV plot. Further, it has been reported that oxide and oxychloride of samarium are electrochemically inactive in the potential window of LiCl-KCl eutectic [64].

The values of E_p^a and E_p^c as functions of concentration are shown in Fig. 3 where each value was the value associated with the third CV scans for a given concentration. It was observed there was no significant influence on E_p^a and E_p^c potentials by the concentration. The electrode potential $E_{1/2}$ was obtained by

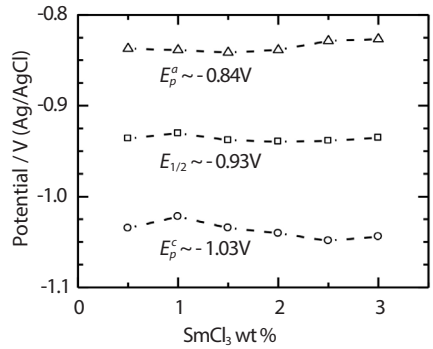

Fig. 3. Potential values of E_p^a and E_p^c as functions of $SmCl_3$ concentration in eutectic LiCl-KCl at 500℃ obtained using a scan rate of 1 $V \cdot s^{-1}$. Included are the calculated values of $E_{1/2}$ as a function of $SmCl_3$ concentration.

$$E_{1/2} = \frac{E_p^a + E_p^c}{2} \quad (3)$$

and is also shown in Fig. 3 as a function of $SmCl_3$ concentration. The values of E_p^a, E_p^c and $E_{1/2}$ for the first EIS experiment were based on the 0.5 wt% CV data and were -0.84, -1.03 and -0.93 V, respectively. These values were used for the remaining EIS experiments as there was consistency in the E_p^a and E_p^c values as shown in Fig. 3. The value of $E_{1/2}$ at -0.93 V was close to the standard potential of the redox Sm^{3+}/Sm^{2+} system in LiCl-KCl that was reported as -0.97 ± 0.02 V relative to Ag/AgCl in literature [27].

The Nyquist and Bode phase angle plots of the EIS data associated with the 1.0 wt% $SmCl_3$ system obtained at a

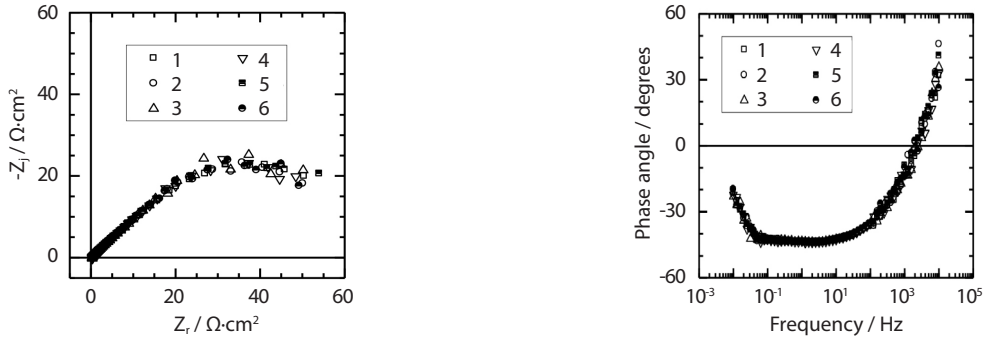

Fig. 4. (a) Nyquist plot and (b) Bode phase angle plot of the six EIS spectra associated with the 1.0 wt% $SmCl_3$ system at 500℃ at a bias potential of -0.93 V relative to a Ag/AgCl reference electrode.

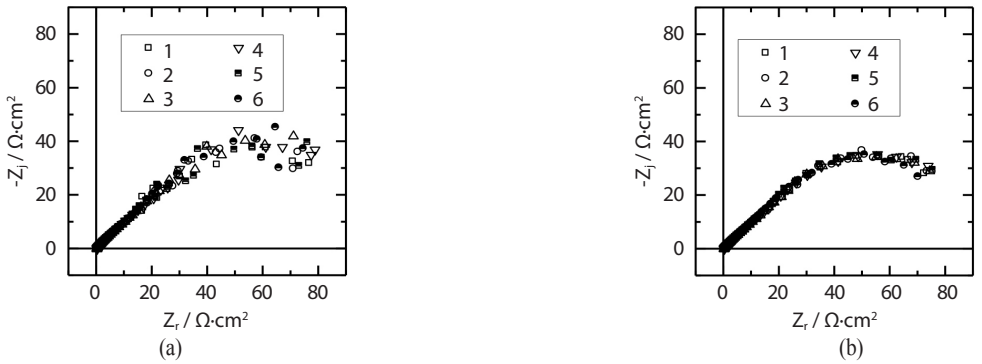

Fig. 5. Nyquist plots of the six EIS spectra associated with the 1.0 wt% $SmCl_3$ in LiCl-KCl at 500℃ at bias potentials of (a) -1.03 V and (b) -0.84 V relative to a Ag/AgCl reference electrode.

bias potential of -0.93 V, $E_{1/2}$, is shown in Fig. 4 for the frequency range of 10 kHz to 0.01 Hz. There was inductive behavior in the high frequency region of the Nyquist plot not easily observed due to scale of the plot, however it is more clearly indicated by the positive phase angle in the Bode phase diagram. There was a small amount of scatter at the low frequency region observed in the Nyquist plot. The repeatability of the EIS spectra is demonstrated by the overlaying of the experimental data as highlighted in the Bode phase angle plot.

Nyquist plots of the EIS data for the 1.0 wt% $SmCl_3$ system are shown in Fig. 5 where the bias potentials were -0.84 V and -1.03 V. These potentials corresponded to the E_p^a and E_p^c, respectively. Inductive loops were present in both data sets although not observable in this figure. The repeatability of the data at the E_p^c potential was demonstrated by overlaying the EIS spectra. There was repeatability of the EIS data down to 0.1 Hz for the E_p^a potential with observable scatter at the low frequency region for frequencies lower than 0.1 Hz. Comparison of the data for the 1.0 wt% $SmCl_3$ system at the E_p^a, E_p^c and $E_{1/2}$ potentials indicated that there was more scatter at low frequencies for the most negative E_p^c potential as compared to the E_p^a and $E_{1/2}$ potentials. This trend was consistent with the different concentrations of $SmCl_3$ investigated.

The Nyquist and Bode phase angle representations of the EIS data associated with spectra obtained at the different concentrations of $SmCl_3$ at a bias potential of -0.93 V

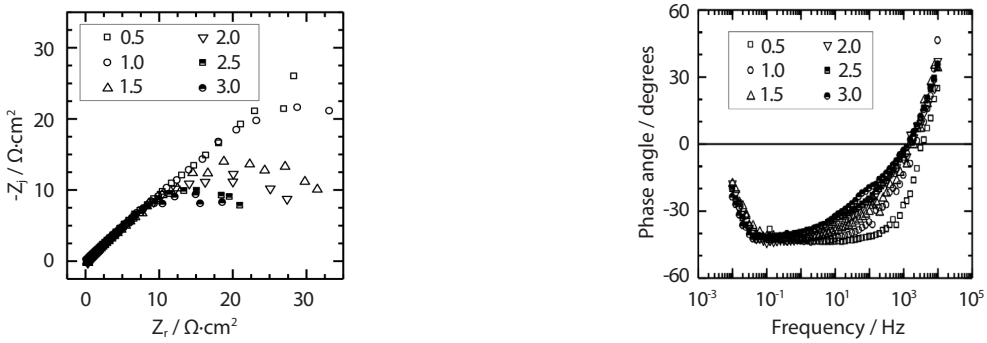

(a) (b)

Fig. 6. (a) Nyquist plot and (b) Bode phase angle plot of the EIS spectra with the concentration of $SmCl_3$ in wt% in eutectic LiCl-KCl at 500℃ as a parameter at a bias potential of -0.93 V relative to a Ag/AgCl reference electrode.

are shown in Fig. 6. A smaller value in the real axis was observed at the low frequency region and was associated with a larger concentration. There was overlay of the data in the Bode phase angle plot at frequencies less than 1 Hz and greater than 1000 Hz. The influence of the concentrations was observable in the frequency range from 1 Hz to 1000 Hz where the response was predominantly capacitive.

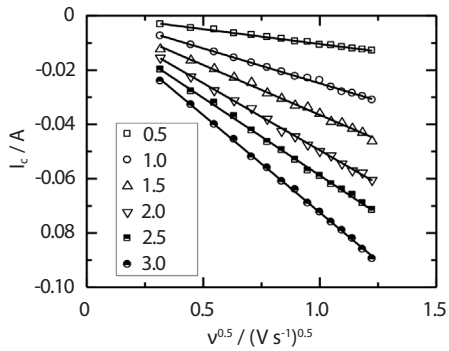

Fig. 7. Plot of cathodic peak current as a function of the square root of scan rate with the concentration of $SmCl_3$ in wt% as a parameter.

4. Discussion

The analysis of the CV and EIS data detailed in this section is focused at demonstrating the applicability of these methods for monitoring the concentration of $SmCl_3$ in the LiCl-KCl eutectic. The CV approach required the calculation of the diffusion coefficient of Sm^{3+}, while the EIS approach required obtaining a relationship between the polarization resistance and the concentration. The diffusion coefficient of the Sm^{3+} ion, $D_{Sm^{3+}}$ was calculated using the Randles-Sevcik equation

$$I_P = 0.4463nFSc_0\left(\frac{nF}{RT}vD\right)^{0.5} \quad (4)$$

where D is the diffusion coefficient ($cm^2 \cdot s^{-1}$), I_p is the cathodic current ($C \cdot s^{-1}$), c_0 is the bulk concentration ($mol \cdot cm^{-3}$), S is the surface area of the electrode (cm^2), and n is the number of electrons transferred, in this case n =1. In this equation F is the Faraday constant ($C \cdot mol^{-1}$), T is the temperature of the electrolyte, which was 500℃ (773 K), and R is the universal gas constant ($J \cdot K \cdot mol^{-1}$). The plot of I_p as a function of $v^{0.5}$ is shown in Fig. 7 with the concentration of $SmCl_3$ as a parameter.

As expected from Equation 4, there was a linear relationship between I_p and $v^{0.5}$ for a given concentration. Linear fits by regression of the data associated with a given concentration yielded the overlaid line on a data set. The slope of a given line was used to calculate the value of $D_{Sm^{3+}}$, shown in Fig. 8. as a function of concentration. The linearity of the curves in Fig. 7 along with the consistency of peak potentials shown in Fig. 2 indicates the system is

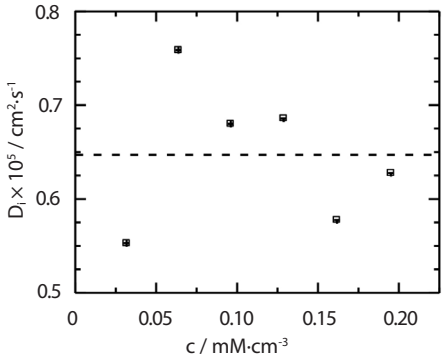

Fig. 8. The diffusion coefficient of Sm^{3+} as a function of the concentration of $SmCl_3$ in LiCl-KCl at 500℃. The horizontal dashed line represents the average value.

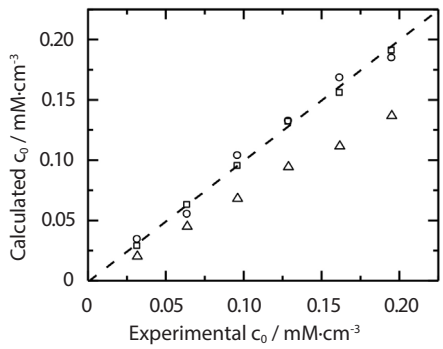

Fig. 9. Calculated bulk concentration values as a function of experimental bulk concentration when using the average (square) and literature (triangle) diffusion coefficients for Sm^{3+} and the polarization resistance-concentration relationship (circle).

reversible and supports the use of Equation 4. The average and standard deviation of the diffusion coefficient, $\bar{D}_{Sm^{3+}}$, for the range of 0.5 to 3.0 wt% (0.03 mmol·cm^{-3} to 0.20 mmol·cm^{-3}) was (0.647 ± 0.076) × 10^{-5} cm^2·s^{-1}. There appears to be no systematic trend with respect to concentration.

The calculated values of the bulk concentration are shown as a function of the experimental c_0 in Fig. 9 for a scan rate of 1 V·s^{-1}. The calculated c_0 values were obtained using Equation 4 together with the $\bar{D}_{Sm^{3+}}$ value and the experimental I_p value associated with a given concentration. There was agreement between the calculated and experimental c_0 values as demonstrated by the proximity of the data points to the diagonal dashed line. The largest error relative to the experimental c_0 values was associated with the lowest concentration at approximately 9% while the relative errors for the other concentrations were less than 2%.

A reported value for the diffusion coefficient of Sm^{3+} ions, $D^*_{Sm^{3+}}$, is 1.30 × 10^{-5} cm^2·s^{-1} that was obtained at a concentration of 0.04 mol·kg^{-1}, approximately 0.065 mmol·cm^{-3}, using a similar CV approach [27]. The asterisk superscript denotes the value of diffusivity was taken from literature. $D^*_{Sm^{3+}}$ was different than the value of $\bar{D}_{Sm^{3+}}$, which is reported here as 0.647 × 10^{-5} cm^2·s^{-1}. It was also significantly different than the value of 0.759 × 10^{-5} cm^2·s^{-1} (reported here) that was associated with a concentration of 0.0637 mmol·cm^{-3}, which is close to that of 0.065 mmol·cm^{-3}. The influence of the literature diffusion coefficient value was investigated by using this value together with the experimental I_p values to calculate c_0 values. These calculated c_0 values are shown as a function of the experimental c_0 values in Fig. 9. It can be seen there was less agreement between the experimental and calculated concentrations with an increase in $SmCl_3$ concentration. The $\bar{D}_{Sm^{3+}}$ value which was calculated using the I_p values associated with concentrations ranging from 0.0317 to 0.195 mmol·cm^{-3} yielded very good agreement between the experimental and calculated bulk concentration values.

It is interesting that the other reported values for $D_{Sm^{3+}}$ at 500℃ and 0.065 mmol·cm^{-3} were 1.41 × 10^{-5} and 0.98 × 10^{-5} cm^2·s^{-1} obtained using semi-integral and CP methods, respectively. This demonstrates the calculation of the diffusion coefficient is sensitive to the experimental method. Also, it is likely that variation in reported diffusion coefficients is a result of the difficulty associated with accurately measuring the true surface area of the working electrode and the concentration of the electrochemically active species at the electrode/electrolyte interface. Table 1 lists values for D found in literature. Although there is no significant influence of the concentration on the calculated value of $D_{Sm^{3+}}$ in this study, the average value $\bar{D}_{Sm^{3+}}$ over the range of concentrations was better suited for use in monitoring concentration changes. These findings suggest it may be

Table 1. Diffusion coefficients for Sm^{3+} at 500℃ calculated by different methods as reported in literature

	Diffusion Coefficient, $D \times 10^5$ $cm^2 \cdot s^{-1}$			
Reference	Convolution	CV	CP	Semi-Integral
27	-	1.30	0.98	1.41
28	-	0.118	-	-
29	1.18 ± 0.26	1.04 ± 0.27	1.01 ± 0.21	-
This Study	-	0.647 ± 0.076 (average)	-	-

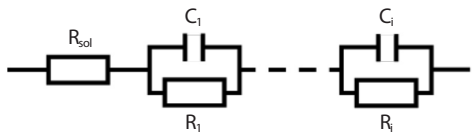

Fig. 10. A schematic representation of a Voigt element equivalent circuit used for analyzing the EIS data.

best practice to determine and utilize a diffusion coefficient that is calculated for a given system rather than relying solely on values from literature.

For the purpose of correlating polarization resistance to concentration of $SmCl_3$, analysis of the EIS data was performed using an equivalent model consisting of a solution resistance in series with several Voigt elements (a measurement model) as shown in Fig. 10. The measurement model method (curve fitting) is a valid approach to implicitly analyze impedance spectra, whereas a process model is phenomena-based [65,66]. In this study, the measurement model was sufficient to estimate the polarization resistance. The model was fitted to data in the range from 0.01 to 1000 Hz where the impedance response is predominantly capacitive.

There was no Warburg element included, as a diffusion-limited process was not observed at the low frequency end of the EIS data. Diffusion effects are usually indicated by a 45-degree line in the low frequency region of a Nyquist plot. The impedance of such a model can be expressed as

$$Z = R_0 + \sum_{i=0}^{n} \frac{R_i}{1 + jw\tau_i} \quad (5)$$

where R_i represents the resistance ($\Omega \cdot cm^{-2}$) for Voigt element i [65]. The characteristic time constant associated with a Voigt element is $\tau_i = R_i C_i$, where C_i is the capacitance (farad) of Voigt element i. The characteristic frequency f_i (Hz) and characteristic time constant are related by $2\pi f_i \tau_i = 1$. The model as shown in Fig. 10 has been used to distinguish between bias and stochastic errors associated with impedance data [67]. The model was used to analyze the EIS data using a complex non-linear least squares algorithm where modulus weighting was used. This involved minimizing the function

$$\chi^2 = \frac{1}{n-m} \sum_{i=1}^{n} \frac{(Z_r(\omega_i;p) - Z_r(\omega_i))^2 + (Z_j(\omega_i;p) - Z_j(\omega_i))^2}{(Z_r^2(\omega_i) + Z_j^2(\omega_i))} \quad (6)$$

where n is the number of data points, m is the number of parameters, and p is the vector of parameters. The variables $Z_r(\omega_i;p)$ and $Z_j(\omega_i;p)$ are the calculated real and imaginary values, respectively, which are functions of the angular frequency ω_i (rad·s^{-1}) and p. The measured real and imaginary values were $Z_r(\omega_i)$ and $Z_j(\omega_i)$, respectively. A down-hill simplex method was used in the regression procedure. Analytical software was written using FORTRAN to analyze the data. The Nyquist and Bode phase angle representations

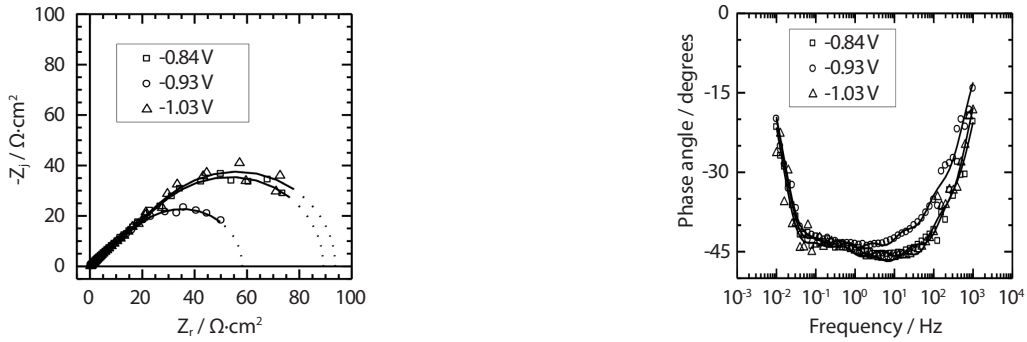

Fig. 11. (a) Nyquist and (b) Bode phase angle plots of EIS data for the 1.0 wt% $SmCl_3$ system with bias potential as a parameter. The solid lines in (a) and (b) that overlay the data represent the fit of the six-element Voigt model to the EIS data and the dotted lines in (a) represent the extrapolation of the given fit to a 0.00001 Hz frequency where the Z_r value is the polarization resistance.

Table 2. Model parameters τ_i and R_i for the fit of the six-element Voigt model to spectrum 2 and the average values $\overline{\tau_i}$ and $\overline{R_i}$ calculated from the model parameters associated with the six spectra for 1.0 wt% $SmCl_3$ system an applied potential of -0.930 V

Element *i* or parameter	Time constant, τ_i (s)	Resistance, R_i ($\Omega \cdot cm^2$)	Average time constant $\overline{\tau_i}$ (s)	Average resistance $\overline{R_i}$ ($\Omega \cdot cm^2$)
1	7.9 ± 0.8	42.6 ± 1.3	8.0 ± 0.3	44.1 ± 1.2
2	1.2 ± 0.34	8.5 ± 1.0	1.1 ± 0.1	8.5 ± 0.4
3	0.22 ± 0.07	4.16 ± 0.66	0.19 ± 0.02	3.85 ± 0.17
4	0.038 ± 0.011	1.71 ± 0.27	0.034 ± 0.004	1.57 ± 0.09
5	(6.0 ± 1.5) ×10^3	0.68 ± 0.10	(5.5 ± 0.6) ×10^3	0.65 ± 0.04
6	(8.2 ± 1.5)×10^4	0.26 ± 0.03	(7.9 ± 0.9) ×10^4	0.23 ± 0.03
R_{sol}	-	0.328 ± 0.006	-	0.326 ± 0.004
R_{polar}	-	58.2	-	59.2 ± 0.9

of the second EIS spectrum associated with the 1.0 wt% $SmCl_3$ system at a bias potential of -0.93 V is shown in Fig. 11. for the frequency range of 1000 Hz to 0.01 Hz.

The optimal fit of the model to the data is included in Fig. 11, where the optimal fit was a six Voigt element model. This was determined by sequentially fitting one, two, three, four, five, six and then seven elements. The agreement between the model and the data improved with each addition of an element. However, the inclusion of a seventh element resulted in parameter errors that included zero. There was good agreement between the six-element model and the data observable in the Nyquist and Bode representations. Regression of the model to the individual measured spectra resulted in chi-squared values that were all less than three ($\chi^2 < 3$). These values of χ^2 compare favorably with the critical value of 35, which is associated with 50 degrees of freedom and 95% probability.

The values of R_i and τ_i listed in Table 2 were obtained from fitting the second EIS spectra for the 1.0 wt% $SmCl_3$ system to the six-element Voigt model. The parameters associated with this model were used to calculate the impedance in the frequency range 0.01 to 0.0001 Hz, thereby extrapolating to the polarization resistance as shown in Fig. 11 by the dotted line. The six spectra associated with

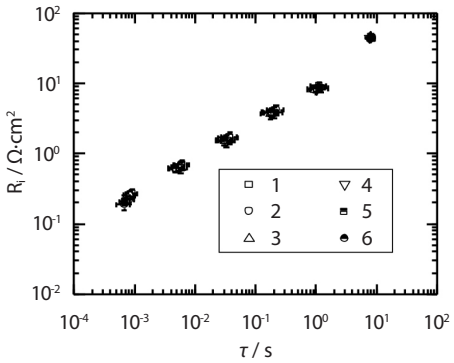

Fig. 12. The R_i value as a function of the τ_i value with the EIS spectrum as a parameter for the 1.0 wt% $SmCl_3$ system. These values were obtained by fitting the EIS spectra to the six-element Voigt equivalent circuit.

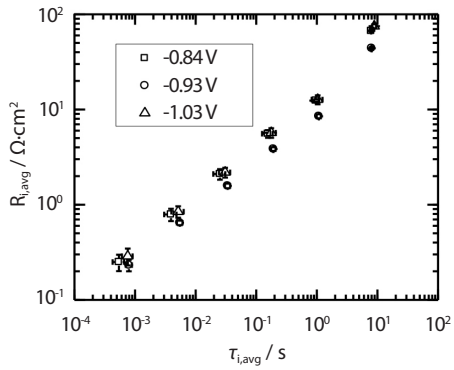

Fig. 13. The $\overline{R}_i$ value as a function of the $\overline{\tau}_i$ value with the applied bias potential as a parameter for the for the EIS data associated with the 1.0 wt% $SmCl_3$ system.

the 1.0 wt% $SmCl_3$ system were each fit to the six-element Voigt model with the R_i values shown in Fig. 12 as a function of the associated values of τ_i where the error bars represent the errors obtained from the regression procedure.

Repeatability was observed of the overlay of R_i values for a given τ_i for the six spectra analyzed. Characterization of the EIS response for a given concentration was given by the average of R_i and τ_i values from the six spectra. The average values $\overline{R}_i$ and $\overline{\tau}_i$ calculated from the six parameter sets associated with the six spectra of the 1.0 wt% $SmCl_3$ system are listed in Table 2 where the standard deviation of a given average value is calculated from the six regressed parameter values.

The Nyquist and Bode phase representations of the EIS data associated with the 1.0 wt% system are shown in Fig. 11 with the applied potential as a parameter. Included is the fit of the six-element Voigt model to each data set and extrapolation to the polarization resistance. The low frequency data for the -1.03 V spectrum was more scattered than the -0.84 V spectrum based on the Nyquist representation. The data for these two spectra overlaid in the Bode phase angle representation. The Bode phase angle representation for the -0.93 V spectrum was different than that of the other applied potentials for frequencies greater than 1 Hz. The $\overline{R}_i$ and $\overline{\tau}_i$ model parameter values obtained from the six spectra associated with the bias potentials of -0.84, -0.93 and -1.03 V are shown in Fig. 13.

The similarity in the EIS response among the three bias potentials was demonstrated in the time constants being approximately the same for a given element. This indicated that the EIS responses of each bias potential was composed of similar line shapes suggesting that the same mechanisms were involved at the three potentials. The influence of the bias potential was observed in the resistor value for elements with a $\overline{\tau}_i$ value greater than 0.5 s where the $\overline{R}_i$ value for the applied $E_{1/2}$ bias potential was less than the values for E_p^c and E_p^a potentials which were similar. This suggested the resistance to any reactions being characterized by the Voigt elements was less at $E_{1/2}$ as compared to E_p^c and E_p^a. This would have been expected as the reversible reaction would be most favorable.

The trend of a smaller $\overline{R}_i$ value for the $E_{1/2}$ bias potential as compared with the E_p^a potential was also observed for the 1.5, 2.0, 2.5 and 3.0 wt% $SmCl_3$ systems. A smaller $\overline{R}_i$ value was associated with a given $\overline{\tau}_i$ value for the EIS data at the E_p^c potential of -1.03 V for the 1 wt% and 1.5 wt% systems. There was scatter in the frequencies less than 0.1 Hz for the systems with higher concentrations and these were not analyzed. The plot of $\overline{R}_p$ as a function of the applied potential with the concentration of $SmCl_3$ as a parameter is shown in

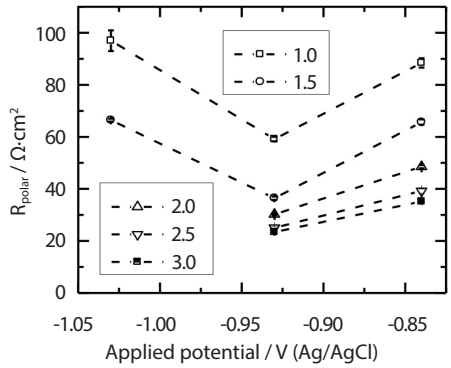

Fig. 14. The average polarization resistance value as a function of bias potential with the $SmCl_3$ concentration in wt% as a parameter.

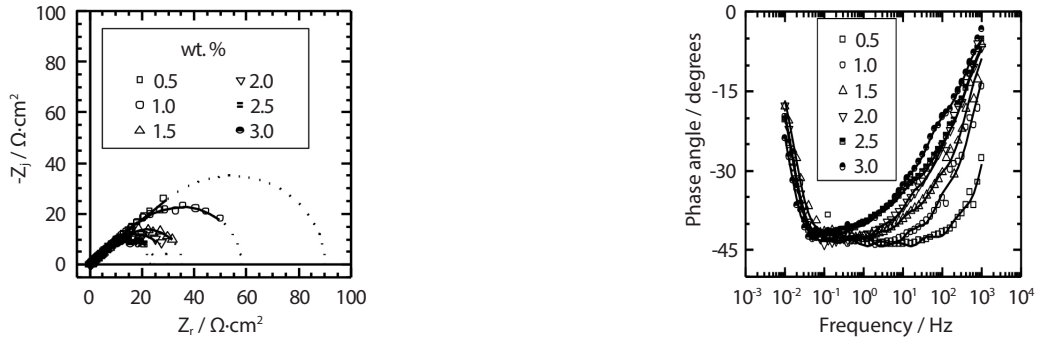

Fig. 15. (a) Nyquist and (b) Bode phase angle plots of EIS data for the $SmCl_3$ system at -0.930 V with the concentration in wt% as a parameter. The solid lines in (a) and (b) that overlay the data represent the fit of the six-element Voigt model to the EIS data and the dotted lines in (a) represent the extrapolation of the given fit to a 0.00001 Hz frequency where the Z_r value is the polarization resistance.

Fig. 14. Each data point represents the average of the six R_p parameters obtained from the six spectra associated with a given condition and the error bar represents one standard deviation.

The EIS data associated with the -1.03 V potential and greater than 1.5 wt% $SmCl_3$ were not analyzed. The $\bar{R}_p$ value was the lowest for the $E_{1/2}$ potential of -0.93 V at 1.0 and 1.5 wt% $SmCl_3$ as compared to the -1.03 V and -0.84 V potentials, E_p^c and E_p^a, respectively. The $\bar{R}_p$ for the $E_{1/2}$ value was lower than the -0.84 V potential for concentrations greater than 1.5 wt % $SmCl_3$. This was consistent where the least resistance was associated with the $E_{1/2}$ bias potential was also observed with the $\bar{R}_i$ parameters.

The Nyquist and Bode phase representations of the EIS data associated with -0.93 V applied potential are shown in Fig. 15 with the concentration of $SmCl_3$ as a parameter. The fit of the six-element Voigt model to each data set is included together with the extrapolation to approximate the polarization resistance.

The EIS data for the 0.5 wt% $SmCl_3$ system was analyzed for the 1000 Hz to 0.1 Hz. The influence of the concentration was seen on the Nyquist plot, where a smaller semicircular loop and R_p value was associated with a larger concentration. The influence of the concentration was observable in the Bode phase angle plot, where for frequencies greater than 0.1 Hz a more negative phase angle was associated

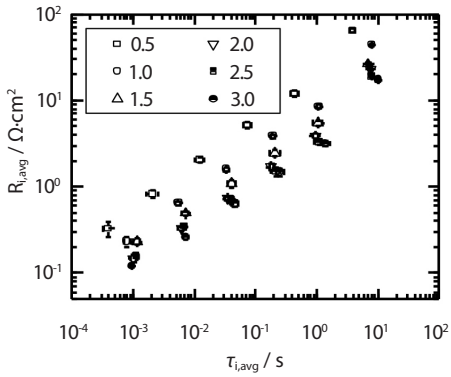

Fig. 16. The $\overline{R}_i$ value as a function of the $\overline{\tau}_i$ value at the bias potential of -0.930 V with the concentration of $SmCl_3$ in wt% as a parameter.

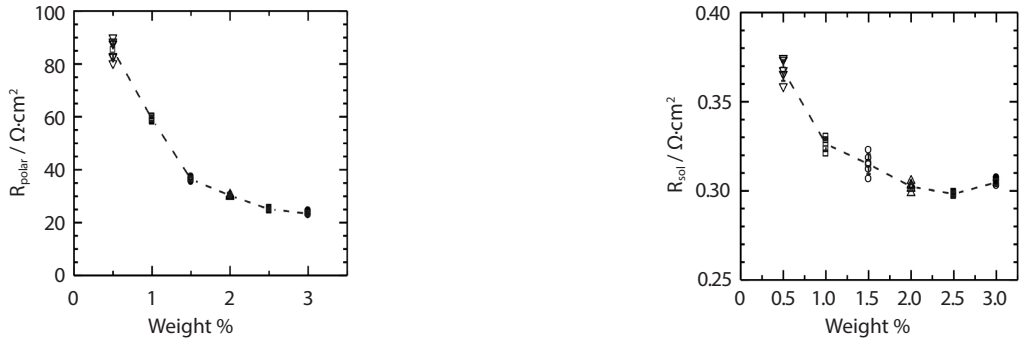

Fig. 17. (a) Polarization and (b) solution resistance values as a function of concentration in wt% $SmCl_3$ associated with the six spectra for a given concentration. The average value of the resistance values as a function of concentration is also included with the dashed lines highlighting the trend associated with these values.

with a larger concentration for a given frequency. The Bode phase angle plot also indicated that the phase angle data at the low frequency end overlaid for frequencies less than 0.1 Hz. The agreement between the six-element Voigt model and the EIS data was demonstrated by the overlay of the model on the data observable both in the Nyquist and Bode phase angle plots.

The value of $\overline{R}_i$ as a function of $\overline{\tau}_i$ is shown in Fig. 16 with concentration as a parameter for the -0.93 V applied potential condition. The $\overline{\tau}_i$ value was approximately equal for a given element except for the values for the 0.5 wt% system, which was slightly less than the value for the other systems for a given element. This indicated that the mechanisms involved in the EIS response were the same for each concentration, as would be expected. Concentration influenced the $\overline{R}_i$ value where a smaller $\overline{R}_i$ value was associated with a larger concentration, for a given element. This indicated that the resistance of a mechanism characterized by an element was less when there was an increase in the concentration, as expected.

The values of R_p and R_{sol} as functions of concentration are shown in Fig. 17(a) and 17(b), respectively. The R_p and R_{sol} values at a given concentration associated with the six spectra obtained for that concentration overlay on each other and are not distinguishable. The larger scatter in the values associated with the 0.5 wt% system was attributed

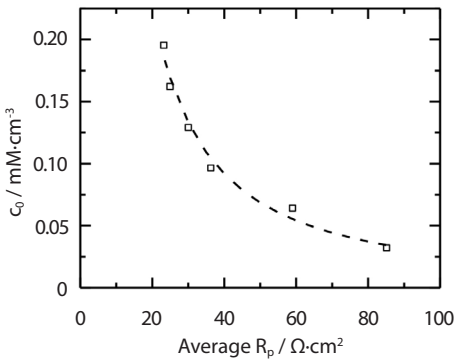

Fig. 18. Experimental bulk concentration value as a function of calculated average polarization resistance. The dashed line is the fit of equation to the data.

to the lowest frequency being measured for these spectra was 0.1 Hz, while for the other concentrations it was 0.01 Hz. Overlaid on these plots are the average values, $\bar{R}_p$ and $\bar{R}_{sol}$, as functions of concentration. It is observed from Fig. 17(a) that there was a monotonic decrease in R_p with concentration as highlighted by the trend associated with the $\bar{R}_p$ values.

A monotonic trend was also observed for the R_{sol} values however, this excluded the largest concentration. The lower value of R_p and R_{sol} associated with a higher concentration was expected. A higher concentration of $SmCl_3$ was more favorable for the reversible reaction with there being a lower resistance exhibited and the solution resistance was lowered due to an increase in ionic conductivity.

The experimental c_0 values were cast as a function of the $\bar{R}_p$ values as shown in Fig. 18 from which an equation of the form

$$c_0 = 0.0111 R_p^{-1.3} \quad (7)$$

was derived by fitting a power function to the data. The $\bar{R}_p$ values associated with a given experimental c_0 values were used to calculate a c_0 values using this equation. The calculated c_0 values were cast as a function of the experimental c_0 value in Fig. 9. There was agreement between the experimental and calculated c_0 values with the relative errors ranging from 3% to 13% for the concentration range investigated.

5. Conclusions

This paper reports both cyclic voltammetry (CV) and electrical impedance spectroscopy (EIS) were effective for the measurement of $SmCl_3$ concentration (0.5 to 3.0 wt%) in molten eutectic LiCl-KCl at 500℃. The CV approach with the Randles-Sevcik equation requires knowledge of the diffusion coefficient, which can either be obtained from the literature or via CV of samples with known concentrations. In this study, an average diffusion coefficient for Sm^{3+} in the salt ($\bar{D}_{Sm^{3+}}$) was determined via the latter approach. For the EIS approach, a polarization resistance/concentration relationship was determined. This demonstrated the consistency of using electrochemical based methods for monitoring the concentration changes in a molten salt such as the LiCl-KCl system. We recommend that an averaged diffusion coefficient of a species in the concentration range should be used for the application of the developed CV approach to concentration estimation. Also, it is recommended for better performance of the developed CV method that diffusion coefficients should be measured experimentally for the given salt matrix rather than relying upon values published in the literature for similar salt matrices. The EIS approach has benefits for implementation, since it does not require an independent measurement of the diffusion coefficient. Note that this study involves a soluble-soluble redox transition. Further study is needed to evaluate the application of EIS to redox transitions with an insoluble reduced species.

6. Acknowledgements

This submitted manuscript was authored by a contractor of the U.S. Government under DOE Contract No. DE-AC07-05ID14517. Accordingly, the U.S. Government

 The experimental work was conducted at the Center for Advanced Energy Studies. The authors gratefully acknowledge the safety and operations support of Kristi Moser-McIntire of Idaho State University and Joanna Taylor of the University of Idaho. A debt of gratitude is owed to Dr. Tae-Sic Yoo for his invaluable advice and thoughtful input.

REFERENCES

[1] I. Johnson, "The Thermodynamics of Pyrochemical Processes for Liquid Metal Reactor Fuel Cycles", J. Nucl. Mater., 154, 169–180 (1988).

[2] J.P. Ackerman, "Chemical Basis for Pyrochemical Reprocessing of Nuclear Fuel", Ind. Eng. Chem. Res., 30, 141–145 (1991).

[3] J.J. Laidler, J.E. Battles, W.E. Miller, J.P. Ackerman, and E.L. Carls, "Development of Pyroprocessing Technology", Prog. Nucl. Energy., 31, 131–140 (1997).

[4] M.F. Simpson, T. Yoo, R.W. Benedict, S. Phongikaroon, S. Frank, P. Sachdev, and K. Hartman, "Strategic Minimization of High-Level Waste from Pyroprocessing of Spent Nuclear Fuel", GLOBAL 2007: Adv. Nucl. Fuel Cycles and Syst., 1394–1397 (2007).

[5] T. Inoue, T. Koyama, and Y. Arai, "State of the Art of Pyroprocessing Technology in Japan", Energy Procedia, 7, 405–413 (2011).

[6] H. Lee, G. Park, K. Kang, J. Hur, J. Kim, D. Ahn, Y. Cho, and E. Kim, "Pyroprocessing Technology Development at KAERI", Nucl. Eng. Technol., 43, 317–328 (2011).

[7] M.A. Williamson and J.L. Willit, "Pyroprocessing Flowsheets for Recycling Used Nuclear Fuel", Nucl. Eng. Technol., 43, 329–334 (2011).

[8] T. Yoo and D.E. Vaden, "A New Inventory Tracking Method for Mark-V Electrorefiner", Ann. Nucl. Energy, 128, 406–413 (2019).

[9] T. Yoo, B.R. Westphal, and K.P. Carney, "Nuclear Material Input Accountancy with a Representative Sampling Method", Ann. Nucl. Energy, 135, 106970 (2020).

[10] A.N. Williams, G.G. Galbreth, and J. Sanders, "Accurate Determination of Density, Surface Tension, and Vessel Depth Using a Triple Bubbler System", J. Ind. Eng. Chem., 63, 149–156 (2018).

[11] J. Kim, J. Lee, S. Bae, S. Paek, S. Kim, T. Kim, and T. Park, "Automated High-Temperature Liquid Level Measurement System Using a Dynamic Tube Pressure Technique", J. Ind. Eng. Chem., 49, 30–35 (2017).

[12] H. Seo, S. Park, B. Won, S. Ahn, H. Shin, S. Na, D. Song, H. Kim, and S. Lee, "Development of a Neutron Measurement System in Unified Non-Destructive Assay for the PRIDE Facility", J. Korean Phys. Soc., 63, 2080–2084 (2013).

[13] M.C. Miller and D.A. Vega, "U.S. Fuel Cycle Technologies R&D Program for Next Generation Nuclear Materials Management", Proc. of Int. Congr. Adv. Nucl. Power Plants, ICAPP 2013 Nucl. Power - A Safe Sustain. Choice Green Futur. Held with 28th KAIF/KNS

Ann. Conf., 869–876 (2013).

[14] T. Koyama, M. Iizuka, Y. Shoji, R. Fujita, H. Tanaka, T. Kobayashiz, and M. Tokiwai, "An Experimental Study of Molten Salt Electrorefining of Uranium Using Solid Iron Cathode and Liquid Cadmium Cathode for Development of Pyrometallurgical Reprocessing", J. Nucl. Sci. Technol., 34, 384–393 (1997).

[15] R.K. Ahluwalia and T.Q. Hua, "Electrotransport of Uranium from a Liquid Cadmium Anode to a Solid Cathode", Nucl. Technol., 140, 41–50 (2002).

[16] S.X. Li, S.D. Herrmann, K.M. Goff, M.F. Simpson, and R.W. Benedict, "Actinide Recovery Experiments with Bench-Scale Liquid Cadmium Cathode in Real Fission Product-Laden Molten Salt", Nucl. Technol., 165, 190–199 (2009).

[17] R.O. Hoover, S. Phongikaroon, S.X. Li, M.F. Simpson, and T. Yoo, "A Computational Model of the Mark-Ⅳ Electrorefiner: Phase I-Fuel Basket/Salt Interface", J. Eng. Gas Turbines Power, 131 (2009).

[18] R.O. Hoover, S. Phongikaroon, M.F. Simpson, S.X. Li, and T. Yoo, "Development of Computational Models for the Mark-Ⅳ Electrorefiner—Effect of Uranium, Plutonium, and Zirconium Dissolution at the Fuel Basket-Salt Interface", Nuc. Technol., 171(3), 276-284 (2010).

[19] Y. Sakamura, M. Iizuka, T. Koyama, S. Kitawaki, and A. Nakayoshi, "Novel Approach to Extracting Transuranic Elements in Molten Salt Electrorefining", Nucl. Technol., 190, 193–206 (2015).

[20] T.Y. Karlsson, G.L. Fredrickson, T. Yoo, D.E. Vaden, M.N. Patterson, and V. Utgikar, "Thermal Analysis of Projected Molten Salt Compositions During FFTF and EBR-Ⅱ Used Nuclear Fuel Processing", J. Nucl. Mater., 520, 87–95 (2019).

[21] P. Masset, D. Bottomley, R. Konings, R. Malmbeck, A. Rodrigues, J. Serp, and J.P. Glatz, "Electrochemistry of Uranium in Molten LiCl-KCl Eutectic", J. of the Electrochem. Soc., 152(6) A1109-A1115 (2005).

[22] P. Masset, R.J.M. Konings, R. Malmbeck, J. Serp, and J.P. Glatz, "Thermochemical Properties of Lanthanides (Ln = La, Nd) and Actinides (An = U, Np, Pu, Am) in the Molten LiCl-KCl Eutectic", J. of Nucl. Mater., 344, 173-179 (2005).

[23] S. Ghosh, S. Vandarkuzhali, N. Gogoi, P. Venkatesh, G. Seenivasan, B. Prabhakara Reddy, and K. Nagarajan, "Anodic Dissolution of U, Zr and U-Zr Alloy and Convolution Voltammetry of $Zr^{4+}|Zr^{2+}$ Couple in Molten LiCl-KCl Eutectic", Electrochem. Acta, 56, 8204-8218 (2011).

[24] R.O. Hoover, M.R. Shaltry, S. Martin, K. Sridharan, and S. Phongikaroon, "Electrochemical Studies and Analysis of 1-10 wt% UCl_3 Concentrations in Molten LiCl-KCl Eutectic", J. of Nucl. Mater., 452, 389-396 (2014).

[25] C.S. Wang, Y. Liu, H. He, F.X. Gao, L.S. Liu, S.W. Chang, J.H. Guo, L. Chang, R.X. Li, and Y.G. Ouyang, "Electrochemical Separation of Uranium and Cerium in Molten LiCl-KCl", J. of Radioanal. and Nucl. Chem., 298, 581-586 (2013).

[26] J. Serp, R.J.M. Konings, R. Malmbeck, J. Rebizant, C. Scheppler, and J.P. Glatz, "Electrochemical Behavior of Plutonium Ion in LiCl-KCl Eutectic Melts", J. of Electroanal. Chem., 561, 143-148 (2004).

[27] G. Cordoba and C. Caravaca, "An Electrochemical Study of Samarium Ions in the Molten Eutectic LiCl+KCl", J. of Electroanal. Chem., 572, 145-151 (2004).

[28] T.-J. Kim, B.O. Jeong, E. H. Lee, D.-H. Ahn, Y. Jung, and S.W. Paek, "Understanding of Electrochemical Reduction of Sm^{3+} in a LiCl-KCl Molten Salt at 773 K", Int. J. of Electrochem. Sci., 7, 11257-11263 (2012).

[29] Y. Castrillejo, C. de la Fuenta, M. Vega, F. de la Rosa, R. Pardo, and E. Barrado, "Cathodic Behavior and Oxoacidity Reaction of Samarium (Ⅲ) in Two Molten Chlorides with Different Acidity Properties: The Eutectic LiCl-KCl and the Equimolar $CaCl_2$-NaCl Melt", Electrochim. Acta, 97, 120-131 (2013).

[30] D. Yoon, J. Pormatikul, M. Shaltry, S. Phongikaroon, and K. Allahar, "Determination of Kinetic Properties

of Sm(Ⅲ)/Sm(Ⅱ) Reaction in LiCl-KCl Molten Salt Using Cyclic Voltammetry and Electrochemical Impedance Spectroscopy", J. of Radioanal. And Nucl. Chem., 322, 2, 1031-1037 (2019).

[31] L. Cassayre, J. Serp, P. Soucek, R. Malmbeck, J. Rebizant, and J.P. Glatz, "Electrochemistry of Thorium in LiCl-KCl Eutectic Melts", Electrochim. Acta, 52, 7432-7437 (2007).

[32] M.R. Bermejo, J. Gomez, J. Medina, A.M. Marinez, and Y. Castrillejo, "The Electrochemistry of Gadolinium in the Eutectic LiCl-KCl on W and Al Electrodes", J. of Electroanal. Chem., 588, 253-266 (2006).

[33] C. Wang, Y. Liu, H. Hi, F. Gao, L. Liu, S. Chang, J. Guo, L. Chang, and Y. Ouyang, "Electrochemical Behavior of Cerium Ion in Molten LiCl-KCl", J. of Rare Earths, 31, 405-409 (2013).

[34] T.J. Kim, D.H. Ahn, S.W. Paek, and Y. Jung, "Study on Electrodeposition of Ce(Ⅲ) at a Tungsten Electrode in a LiCl-KCl Molten Salt Solution", Int. J. of Electrochem. Sci., 8, 9180-9186 (2013).

[35] K.C. Marsden and B. Pesic, "Evaluation of the Electrochemical Behavior of $CeCl_3$ in Molten LiCl-KCl Eutectic Utilizing Metallic Ce as an Anode", J. of the Electrochem. Soc., 158(6), F111-F120 (2011).

[36] Y. Castrillejo, M.R. Bermejo, E. Barrado, and A.M. Martinez, "Electrochemical Behaviour of Erbium in the Eutectic LiCl-KCl at W and Al Electrodes", Electrochim. Acta, 51, 1941-1951 (2006).

[37] P. Masset, C. Apostolidis, R.J.M. Konings, R. Malmbeck, J. Rebizant, J. Serp, and J.-P. Glatz, "Electrochemical Behaviour of Neptunium in the Molten LiCl-KCl Eutectic", J. of Electroanal. Chem., 603, 166-174 (2007).

[38] D. Vaden, "Fuel Conditioning Facility Electrorefiner Model Predictions Versus Measurements", Sep. Sci. Technol., 43, 2684-2694 (2008).

[39] R.A. Borrelli, "Use of Curium Neutron Flux from Head-End Pyroprocessing Subsystems for the High Reliability Safeguards Methodology", Nucl. Eng. Des., 277, 166–172 (2014).

[40] D. Rappleye, S. Jeong, and M. Simpson, "Application of Multivariate Analysis Techniques to Safeguards of the Electrochemical Treatment of Used Nuclear Fuel", Ann. Nucl. Energy, 77, 265–272 (2015).

[41] X.-Z. Yuan, C. Song, H. Wang, and J. Zhang, Electrochemical Impedance Spectroscopy in PEM Fuel Cells: Fundamentals and Applications, Springer, London (2010).

[42] V. Encinas-Sanchez, M.T. de Miguel, M.I. Lasanta, G. Garcia-Martin, and F.J. Perez, "Electrochemical Impedance Spectroscopy (EIS): An Efficient Technique for Monitoring Corrosion Processes in Molten Salt Environments in CSP Applications", Sol. Energy Mater. and Sol. Cells, 191, 157-163 (2019).

[43] B.J. Merten, Coating Evaluation by Electrochemical Impedance Spectroscopy, United States Bureau of Reclamation Report, ST-2016-7673-1 (2015).

[44] D.D. MacDonald, "Review of Mechanistic Analysis by Electrochemical Impedance Spectroscopy", Electrochim. Acta, 35, 1509-1525 (1990).

[45] A. Kisza and J. Kazmierczak, "Kinetics of Electrode Reactions on Metallic Electrodes in Pure Molten Chlorides", Chem. Papers, 45, 187-194 (1991).

[46] S.A. Kuznetsov and M. Gaune-Escard, "Electrochemical Transient Techniques for Study of the Electrochemistry and Thermodynamics of Nuclear Materials in Molten Salts", J. Nucl. Mater., 389, 108-114 (2009).

[47] H. Tao and B. Pesic, "Electrochemical Behavior of $LaCl_3$ and Morphology of La Deposit on Molybdenum Substrate in Molten LiCl-KCl Eutectic Salt", Electrochim. Acta, 119, 120-130 (2014).

[48] G. Salinas-Solano, J. Porcayo-Calderon, J.G. Gonzalez-Rodriguez, V.M. Salinas-Bravo, J.A. Ascencio-Gutierrez, and L. Martinez-Gomez, "High Temperature Corrosion of Inconel 600 in NaCl-KCl Molten Salts", Adv. Mater. Sci. Eng., 2014, 696081 (2014).

[49] J.L. Trinstancho-Reyes, M. Sanchez-Carrillo, R. Sandoval-Jabalera, V.M. Orozco-Carmona, F. Almeraya-Calderon, J.G. Chacon-Nava, J.G. Gonzalez-Rodriguez,

and A. Martinez-Villafane, "Electrochemical Impedance Spectroscopy Investigation of Alloy Inconel 718 in Molten Salts at High Temperature", Int. J. Electrochem. Sci., 6, 419-431 (2011).

[50] M. Misra, K.S. Raja, and J. Ruppert, "Electrochemical Corrosion Behavior of Refractory Metals in LiCl-Li_2O Molten Salt", ECS Trans., 33, 181-192 (2010).

[51] J.-Y. Kim, Y.S. Choi, S.-E. Bae, I. Yum, D.H. Kim, J.-W. Yeon, and K. Song, "Electrical Conductivity Measurement of Molten Salts Using a Two-Electrode Alternative Current Impedance Method", Asian J. Chem., 25, 7028-7030 (2013).

[52] U. Stohr and W. Freyland, "Electrochemical Impedance Investigations of Redox Mechanisms of Refractory Metal Compounds in Molten Salts. I. Niobium Chloride and Oxychloride in CsCl-NaCl Eutectic Melt", Electrochim. Acta, 44, 2199-2207 (1999).

[53] Z. Chen, J. Liu, Z. Yu, and K.C. Chuo, "Electrical Conductivity of $CaCl_2$-KCl-NaCl System at 1080 K", Thermochim. Acta, 543, 107-112 (2012).

[54] S.A. Kuznetsov and M. Gaune-Escard, "Electronic Conductivity of NaCl-KCl Equimolar Melt Containing Eu(Ⅲ) and Eu(Ⅱ) Complexes by Electrochemical Impedance Spectroscopy", Z. Naturforsch., 61a, 486-490 (2006).

[55] E.V. Kirillova and V.P. Stepanov, "Capacitance of the Double Electrical Layer on the Copper-Group Metals in Molten Alkali Metal Halides", Russ. Metall., 2016, 691-697 (2016).

[56] A. Kisza, "The Capacitance of the Diffuse Layer of Electric Double Layer of Electrodes in Molten Salt", Electrochim. Acta, 51, 2315-2321 (2006).

[57] D. Rappleye and M.F. Simpson, "Application of the Rotating Cylinder Electrode in Molten LiCl-KCl Eutectic Containing Uranium(Ⅲ)- and Magnesium(Ⅱ)-Chloride", J. Nucl. Mater., 487, 362-372 (2017).

[58] D. Yoon and S. Phongikaroon, "Electrochemical Properties and Salt Analyses of $CeCl_3$ in LiCl-KCl Eutectic Salt", J. Electrochem. Soc., 162, E237-E243 (2015).

[59] S. Guo, E. Wu, and J. Zhang, "Exchange Current Density of Gd(Ⅲ)/Gd Reaction in LiCl-KCl Eutectic and Analysis of Errors Caused by Various Methods ", Electrochim. Acta, 259, 253-261 (2018).

[60] B. Prabhakara Reddy, S. Vandarkuzhali, T. Subramanian, and P. Venkatesh, "Electrochemical Studies on the Redox Mechanism of Uranium Chloride in Molten LiCl-KCl Eutectic", Electrochim. Acta, 49, 2471-2478 (2004).

[61] S. Ghosh, S. Vandarkuzhali, P. Venkatesh, G. Seenivasan, T. Subramanian, B. Prabhakara Reddy, and K. Nagarajan, "Redox Behavior of Cerium Oxychloride in Molten $MgCl_2$-NaCl-KCl Eutectic", Electrochim. Acta, 52, 1206-1212 (2006).

[62] S. Vandarkuzhali, N. Gogoi, S. Ghosh, B. Prabhakara Reddy, and K. Nagarajan, "Electrochemical Behaviour of $LaCl_3$ at Tungsten and Aluminium Cathodes in LiCl-KCl Eutectic Melt", Electrochim. Acta, 59, 245-255 (2012).

[63] D.M. Ferry and G.S. Picard, "Impedance Spectroscopy of the Ti(Ⅳ)/Ti(Ⅲ) Redox Couple in the Molten LiCl-KCl Eutectic Melt at 470℃", J. of Appl. Electrochem., 20, 125-131 (1990).

[64] K. Liu, Y.L. Liu, L.Y. Yuan, H. He, Z.Y. Yang, X.L. Zhao, Z.F. Chai, and W.Q. Shi, "Electroextraction of Samarium from Sm_2O_3 in Chloride Melts", Electrochim. Acta, 129, 401-409 (2014).

[65] P. Agarwal, M.E. Orazem, and L.H. Garcia-Rubio, "Measurement Models for Electrochemical Impedance Spectroscopy", J. Electrochem. Soc., 139, 1917-1927 (1992).

[66] P. Zoltowski, "A New Approach to Measurement Modelling in Electrochemical Impedance Spectroscopy", J. Electroanal. Chem., 375, 45-57 (1994).

[67] K.N. Allahar, M.E. Orazem, D.P. Butt, H.A. Chin, W. Ogden, and R. Yungk, "Impedance of Steels in New and Degraded Ester Based Lubricating Oil", Electrochim. Acta, 51(8-9), 1497-1504 (2006).